

Article

# Towards Airborne Thermography via Low-Cost Thermopile Infrared Sensors

João Valente <sup>1,\*</sup>, Juan Jesús Roldán <sup>2</sup>, Mario Garzón <sup>3</sup> and Antonio Barrientos <sup>2</sup>

<sup>1</sup> Information Technology Group, Wageningen University & Research, 6708 PB Wageningen, The Netherlands

<sup>2</sup> Centre for Automation and Robotics (UPM-CSIC), Technical University of Madrid, 28006 Madrid, Spain; jj.roldan@upm.es (J.J.R.); antonio.barrientos@upm.es (A.B.)

<sup>3</sup> Université Grenoble Alpes, Inria, Grenoble INP, 38000 Grenoble, France; ma.garzon@upm.es

\* Correspondence: joao.valente@wur.nl; Tel.: +31-628-398-164

Received: 2 February 2019; Accepted: 19 March 2019; Published: 24 March 2019



**Abstract:** This paper presents a novel tool capable of collecting thermal signatures inside a building by using low-cost IR temperature sensors mounted on-board an aerial platform. The proposed system aims to facilitate the detection of heat loss inside buildings, which is a key aspect for improving energy efficiency in large commercial or industrial buildings. Current detection systems usually require manual labor as well as the use of expensive instrumentation. The proposed system on the other hand, relies on the use of a small unmanned aerial vehicle carrying low-cost thermopile IR sensors. Moreover, the system delivers a fast temperature sensing scheme and it provides coverage to inaccessible areas, thus overcoming the limitations of current mobile platforms which use ground robots. Different experiments were carried out in order to assess the behavior of the sensors as well as to validate the full system. Moreover, the hypothesis that thermopile IR sensors can be used to track temperature signature on-the-fly is validated experimentally with the use of the proposed system over different targets.

**Keywords:** unmanned aerial vehicle; temperature tracking; IR temperature sensors; aerial remote sensing; energy efficiency

## 1. Introduction

Environmental protection and conservation has been a matter of high concern for many public and private entities in the past decades, as a response of these concerns, many government agencies have developed and implemented action plans so as to overcome or correctly manage different environmental challenges [1]. Those plans are oriented, among many other aspects, to improve the lifetime of energetic resources, also to reduce misspent energy, and to increase the quality of pollution control techniques. Moreover, one of the most important, environment-oriented, challenges nowadays is the improvement of energy efficiency in buildings and other infrastructures [2]. These challenge of reducing of misspent energy in buildings is the motivation behind the development of the system presented in this paper, which intends to develop an autonomous remote sensing platform capable of monitoring and mapping heat losses in large buildings.

In the European Union, buildings account for 40% of energy consumption and 36% of CO<sub>2</sub> emissions, in order to wade into this issue, in June of 2018, the Council of the European Union published the amending Energy Performance of Buildings Directive (2018/844/EU), this directive requires state members to define a strategy to improve Europe's energy saving and de-carbonization by 2050 [3]. One of the strategies that can help to achieve the goals of the aforementioned directive, is the detection of energy losses in large non-residential infrastructures. Furthermore, with this objective in mind, the continuous inspection and monitoring systems become essential steps towards the setting

up of autonomous energy control systems that can improve the energetic efficiency in those type of buildings.

In many industrial and commercial buildings, the continuous heating and cooling airflow cycles constitute a critical source of energy waste [4]. In order to overcome this problem, different energy monitoring methodologies have been applied, both outside and inside buildings. One of the main techniques used is the creation of thermal maps from specific sites of the building. These maps can be used by experts to perform post hoc analysis and to design energy efficiency strategies. The system presented in this paper proposes a novel approach to these tasks, by developing an aerial autonomous remote sensing platform, which is capable of monitoring and mapping heat losses in large buildings.

Remote sensing practices have improved significantly with the adoption of Unmanned Aerial Vehicle (UAV) equipped with color and false color cameras [5–7]. Nevertheless, thermal imaging or thermography, with these small UAV is only emerging and there is room for improvements, thus making the proposed system a relevant development.

The most common approach for monitoring the energy of a building, is taking images from outside the building using a UAV equipped with a high-resolution thermal camera. Several views can be used to get temperature profiles [8]. Another example is found in the work of Aguilera et al. that proposes a system capable of generating thermographic 3D models as well as orthoimages in order to assess energy efficiency in buildings facades [9].

Regarding indoor energy-aware applications, most of them rely on static sensors monitoring [10], manual measuring [11], or mobile sensor platforms [12]. Finally, when it comes to continuous monitoring or exploring the building, an autonomous robot with the appropriate sensors can be a suitable solution [13]. A mobile sensor platform denoted as Irma3D, which carries a thermal camera and a laser scanner is used for building indoor 3D heat distribution and flow models [12]. Mobile platforms have been applied to more specific environments as well, for example, a robot named THOMAS was used for temperature monitoring in data centers [14]. The robot is made up with inexpensive chassis and carries a conventional digital camera and a thermocouple interface.

In this paper, a novel approach to the continuous monitoring is presented, it is based on the use of an Aerial Remote Sensing System (ARSS) equipped with several low-cost Infra-Red (IR) temperature sensors. It was developed in order to advance in the supervision of energy efficiency with autonomous remote sensing platforms. This work explores an scenario where high resolution thermography is not a requirement. Furthermore, this prototype was designed to aid critical energy-aware buildings, such as a data center. This type of infrastructure consumes much more energy than standard office workspaces and there is usually a large margin for energy efficiency improvement with adequate temperature monitoring [15].

A comparative between the existing thermography assessment approaches is given in Table 1. This qualitative analysis focus on the human effort, completion time, return of investment (ROI), area coverage by the sensing systems, accuracy of the sensors, spatial resolution achieved, and price of the instrumentation. The detailed ROI analysis of manual and automated methods is provided in Appendix A.

The main contributions of this work are: (1) Design and experimentally validate a novel Software-Hardware (SW/HW) architecture for measuring and processing temperature data; (2) to prove the hypothesis that the MLX90614 infrared sensors can be placed in an aerial platform for measuring temperature in a real-time flight; and (3) to investigate if high changes of temperature could be detected on the fly using the combination of airborne and IR temperature sensors.

**Table 1.** Comparison of different cost/effort per thermography approach found in literature. The crosses used for qualifying the costs can be read as: (+) less costly, (++) costly, and (+++) very costly.

		Automated			
		Manual	Fix Cameras	UGV	UAV
Cost/Effort	Human effort	+++	+	++	++
	Time	+++	+	++	++
	ROI	+++	+++	+	++
	Area coverage	+++	+++	++	+
	Accuracy	+	+	+++	++
	Spatial resolution	+	+	+++	++
	Sensors	+++	+++	+	+

## 2. Proposed Approach

This section describes the proposed approach, it starts with a brief description of the overall approach, then the UAV and sensors used for the system are detailed, and finally, the software developed is explained.

### 2.1. Overall Approach

As aforementioned, the proposed system is based on the use of an ARSS equipped with several IR thermal sensors. This approach allows to track temperature signatures inside buildings because of its high-maneuverability, as well as its ability to perform vertical take-off and land in small areas.

The system is complemented with a specifically designed software, which allows to control and collect the measurements of the sensors, perform filtering and also to combine this information with the other systems running on the main computer of the ARSS.

### 2.2. Aerial Platform

The aerial platform selected is the Ascending Technologies quad-rotor *Pelican*, which is suitable for indoor environments. This UAV is characterized by its robustness among the small quad-rotor systems. Its minimum take-off weight is 630 g and its maximum payload is 500 g. It can fly up to 20 min depending on the payload. The *Pelican* is also easily configurable due to a central main frame made of balsam wood where several carbon plates can be placed, thus facilitating the incorporation of additional devices and sensors.

The *Pelican* is equipped with a 2.1 GHz quad-core processor, 4 GB of RAM, and an autopilot board. The autopilot contains 2 ARM7 micro-controllers, an Inertial Measurement Unit (IMU), and a pressure sensor. An additional Arduino Nano was used for the low-level sensors interface, i.e., temperature and ultrasonic distance sensor used to measure the quad-rotor height above the ground. Finally, the indoor coordinates can be delivered by the system proposed by Dryanovski et al. [16]. The complete ARSS payload, including some additional power and control boards, is presented in Table 2.

**Table 2.** ARSS payload discriminated.

Device	Weight	Quantity
Atomboard and control board	220 g	1
Yellow propeller protection	29 g	2
Arduino Nano	6 g	1
Arduino support	12 g	1
I2C and power connection board	9 g	1
MLX sensor board	12 g	5
MaxSonar sensor	4 g	1
Total	292 g	12

### 2.3. Thermal Sensors

The temperature sensors from the ARSS were selected based on three requisites: the sensors must be able to measure temperature remotely, have a low weight, be economically affordable, and provide an increased accuracy. The temperature sensors that were found to sum up all those characteristics are the IR thermopile sensors, e.g., the models MLX90614. The IR sensor measures the surface temperature of an object when pointing towards it via its thermal radiation. This phenomenon is explained by the fact that all the objects with a  $T > 0$  K emit a continuously thermal radiation [17]. The radiation emitted by the object is detected by the IR sensor that converts it in voltage, and later in temperature. This relationship is known by the Stefan–Boltzmann power radiated law and is given by:

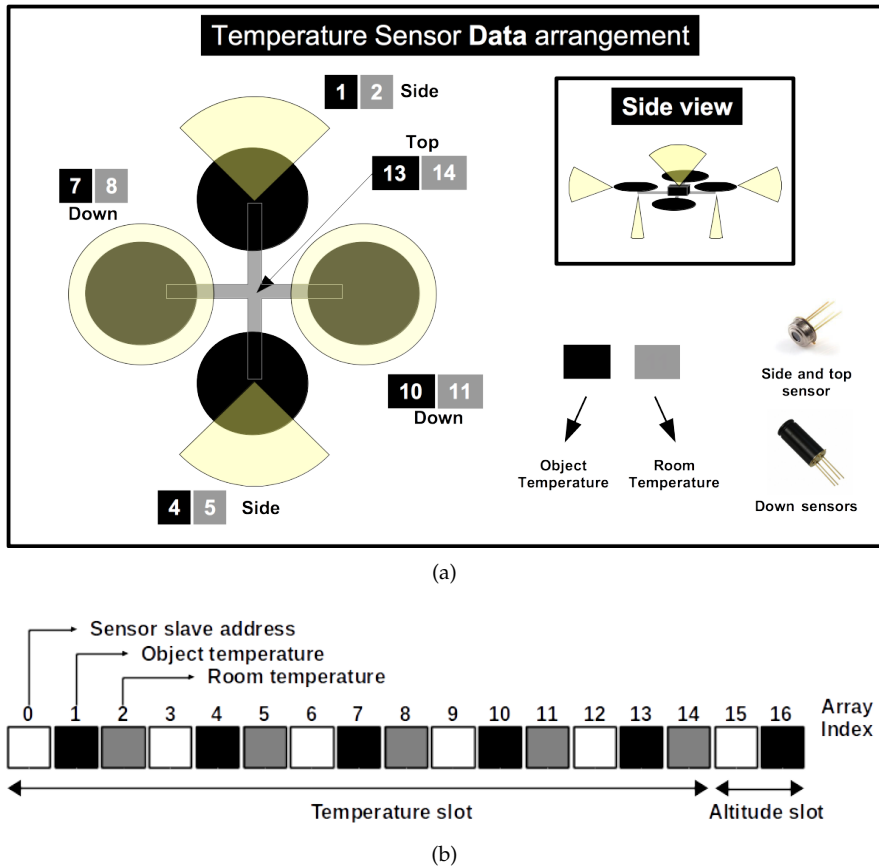
$$P = A\varepsilon\sigma T^4,$$

where  $A$  is the area of the surface radiated,  $\varepsilon$  is the emissivity value that ranges from 0.0 to 1.0,  $\sigma$  is the Stefan–Boltzmann constant ( $5.670367 \times 10^{-8} \text{ Wm}^{-2}\text{K}^{-4}$ ), and  $T$  is the object temperature. The two main parameters of IR sensors are: Field of View (FoV) and Distance from the Object (DO). The sensors field-of-view should be enough to cover the whole object surface at an affordable distance-from-the-object, because the temperature readings are an average of the temperature covered by the sensor. The emissivities of the surfaces should be provided to the data processing algorithm in order to obtain more accurate measurements. In this work, we have considered a constant value for emissivity of 0.95, since most of the used materials present closer values. However, if the system is deployed in a specific scenario with a defined purpose, these emissivity values should be adjusted taking into account the target materials.

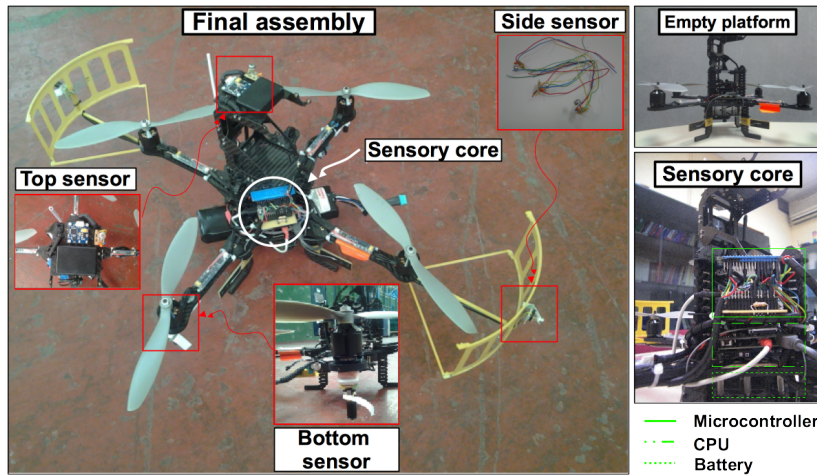
The MLX90614 is a non-contact IR temperature sensor with a thermopile chip made by an array of thermal elements. The sensor is hermetically sealed into a TO-39 metal housing. The MLX90614 is factory calibrated for an object emissivity of 1. This parameter can be customized without any further calibration and black body. Moreover, the sensor provides two temperature readings: object and room (ambient). It can measure a wide range of temperatures with resolution up to  $0.02^\circ\text{C}$ . The maximum—object and room—accuracy that can be achieved is  $0.5^\circ\text{C}$  from temperatures measurements ranging from  $0.0^\circ\text{C}$  to  $50^\circ\text{C}$ . Finally, an integrated SMBus provides a fast interface for building up a temperature sensor network [18].

Figure 1 shows a representation of the temperature sensing arrangement on-board the UAV. As can be observed, two different model thermal sensors (MLX90614) are used, the offer a FoV of  $90^\circ$  and  $10^\circ$ , respectively. The system must be able to measure data in all directions. Therefore, it is desirable to have the sensors set up on the edges of the robot as far as possible from each other, symmetrical (opposed arms of the quad-rotor) and pointing upwards and downwards.

The following configuration has been selected: one  $90^\circ$  FoV sensor on the top of the tower of the Pelican to measure the temperature upwards (called 13 and 14) and two  $10^\circ$  FoV sensors oriented to the ground—one on the left arm and one on the right arm (named 7, 8, 10 and 11). These sensors enable the monitoring of surfaces that are under the ARSS. On the sides there are two  $90^\circ$  FoV sensors (named 1, 2, 4 and 5). The sensors are placed on the plastic protections from the arms to measure the temperature on the ARSS sides (see Figure 2).



**Figure 1.** The MLX90614 sensors: (a) Sensor arrangement and identification number in the quad-rotor frame; (b) The message sent by the node for temperature is an array of floats, including all the measurements read by the Arduino board during a loop, i.e., temperature and sonar readings.



**Figure 2.** On-board sensors and processing units arrangement. The payload system was approximately 700 g.

2.4. Software

Finally, all the software necessary to manage the ARSS middleware is open source and ROS-based [19]. A node has been implemented to address the graphical representation of the temperature values over the robot position on the workspace. This is the node that is responsible for creating a map of temperatures. One of its functions is to establish a range for each RGB color temperature linearly. Thus, the node receives a temperature and a position given by the robot and

issues a color and a position to be represented. The diagram that shows the nodes and topics that address the temperature readings and mapping is shown in Figure 3.

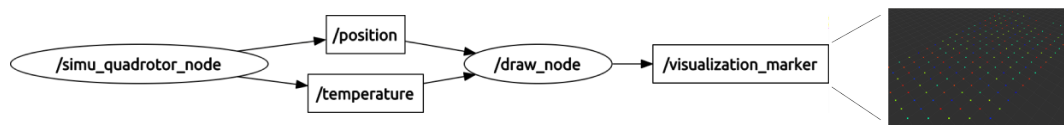


Figure 3. ROS node for temperature mapping.

### 3. Experiments and Results

In order to test the SW/HW system architecture described in Section 2, several tests were performed inside a building, during this experiments the UAV was manually controlled by an experienced pilot. The main objective of the tests is to validate the real-time data acquisition of both the omni-directional temperature and the flying height. Moreover, the test will also allow us to determine that there is not any significant electromechanical noise (i.e., discrete high/low temperature peaks) in the readings.

#### 3.1. System Behavior Assessment

In the first experiment the relationship between the Sensor Coverage (SC) and the Distance from the Object (DO) was analyzed. The experiments were carried out by using a surface with 1 m<sup>2</sup> that was heated up to 37 °C (as measured with an additional hand-held sensor). The DO ranged from 50 cm to 400 cm.

As aforementioned, one measurement value is given by the average of all the internal temperature points from the sensor. Therefore, the object or surface temperature measurement will be more accurate if the Object Length (OL) is larger than the Sensor Coverage at a determinate Distance from the Object. If the OL is smaller than the SC, then the internal sensor’s average readings will also include environment temperature measurements, which are usually lower. This produces a measurement that does not exactly corresponds to the actual temperature of the object that is being measured. Therefore, the DO must becomes one very important aspect to be taken into account when inspecting a building. The relationship between SC and DO is shown in the upper left image from Figure 4. For instance, the SC will be less than 1 m when the DO with the 90° sensor is less than 40 cm, and the DO with the 10° sensor is less than 400 cm, orange circles on the left image represent environmental temperature data that can affect the accuracy of the readings.

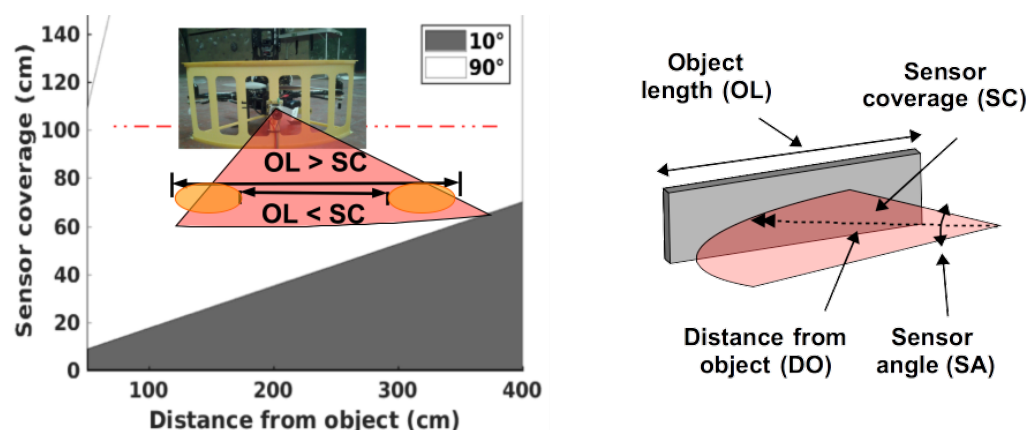
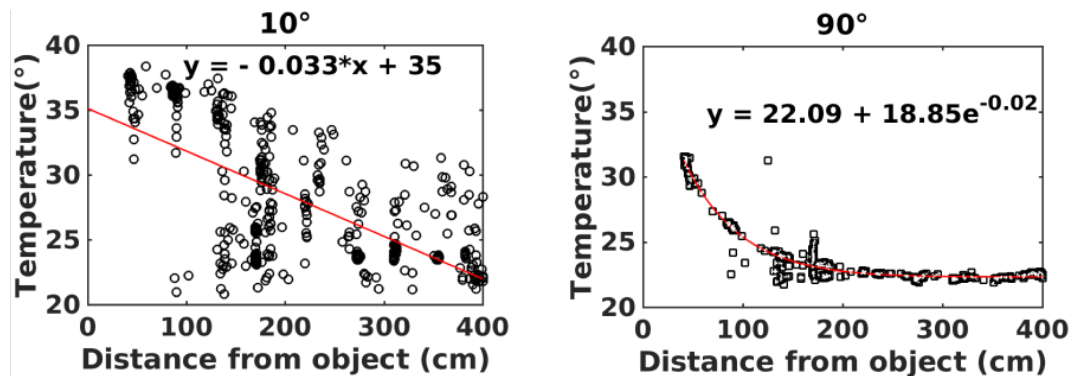


Figure 4. Relationship between Object Length (OL), Sensor Coverage (SC) and Distance from the Object (DO).

When measuring with 10° sensors the temperature readings will be less affected if the DO increases. This behavior is shown in the Figure 5, which depicts the temperature versus DO relationship. It can also be noticed that the temperature drops linearly with the 10° sensor, and exponentially with the 90° sensor. Consequently, the object temperature error will increase faster with the 90° sensor than with the 10° when the ARSS moves away from the object.



**Figure 5.** MLX90614 assessment—10° and 90°—sensors, versus the sensing distance. The object employed has a heated (37 °C) surface of 1 m length. The mean and standard deviation of the environment temperature measured by sensors with 10° and 90° of FoV is respectively,  $24.36 \pm 0.18$ , and  $25.22 \pm 0.22$ .

From the results of is experiment, it can be observed that the 10° sensor provides more accurate measurements when measuring smaller surfaces. However, if the target object has a large surface, such as a roofs or a wall, the 90° will perform good as well.

### 3.2. Full Platform Validation

The second set of experiments are oriented ot validate the overall performance of the proposed system. To achieve this, the platform was validated in indoor scenarios by measuring the temperature values that are above, below and in front the platform during a real-time flight. Two different tests were carried out, during the first one, the UAV was maneuvered close to some pedestrians, whereas for the second one, the platform flew over a warm electrical device. In both cases, the temperature profiles were obtained for every sensor on-board the platform, the positioning and labeling of each sensor is described in Section 2.3.

Figure 6 shows the measurements as the platform takes off and moves near some pedestrians. It can be observed how room temperatures start to increase during take-off (sensors 2, 5, 8, 11 and 14). A dashed rectangular area shows the time lapse when the UAV flew up to 2 m above the ground. This thermodynamic behavior is well known and can be recorded inside any building. Moreover, during this test, the bottom image shows several temperature peaks (i.e., data[4] in Figure 6 legend). Those measurements correspond to a side sensor pointing towards pedestrians located nearby, at distances up to 3 m.

The second test involved some more advanced maneuvers. In this case, the UAV flew over a mobile robot with several working equipment, this robot has therefore a warm cover that was used as the main object to be measured. The measurements obtained during this tests are presented in Figure 7. It can be observed that as when the UAV hovered over the platform the sensors pointing down (7 and 10) indicate that an object with a high temperature was found below the platform. The images acquired by the on-board camera in the time frame 14.3–34.9 s are shown in Figure 8.

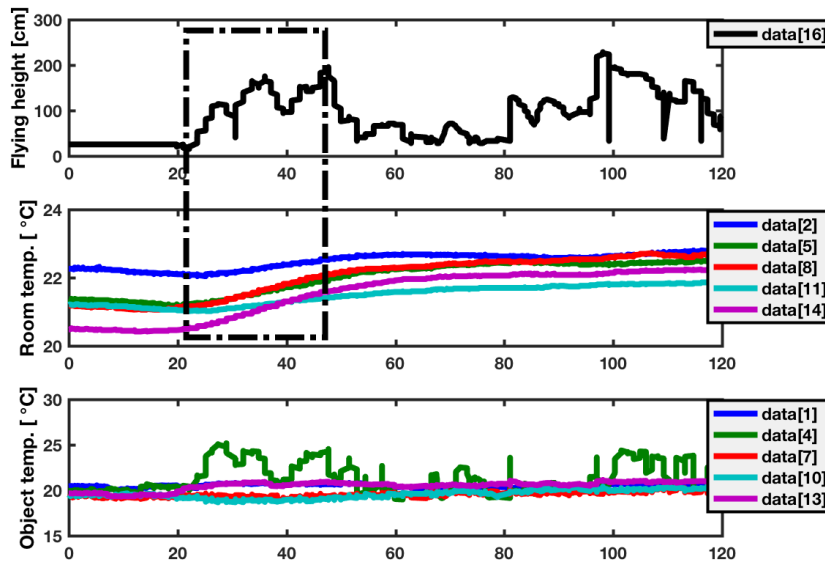


Figure 6. Multiple temperature measurements—room and object—and quad-rotor height from the floor acquired during a real-time flight versus the time.

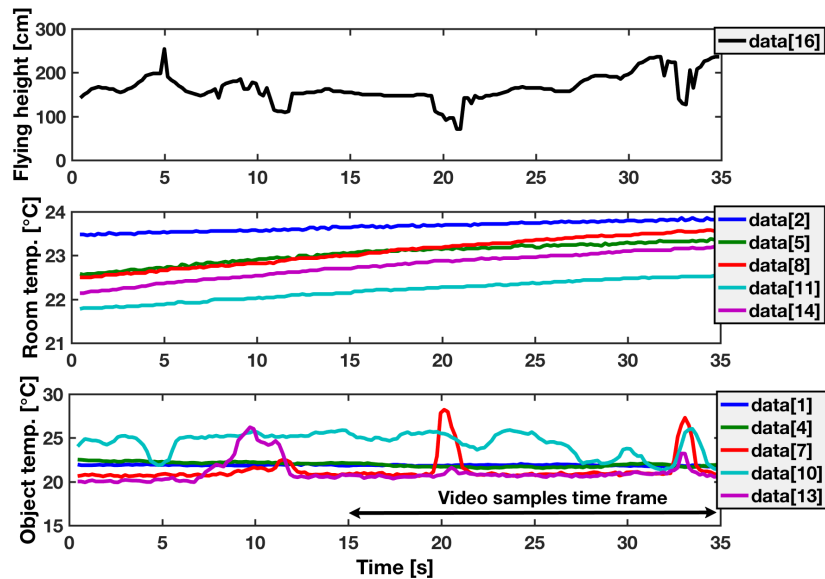


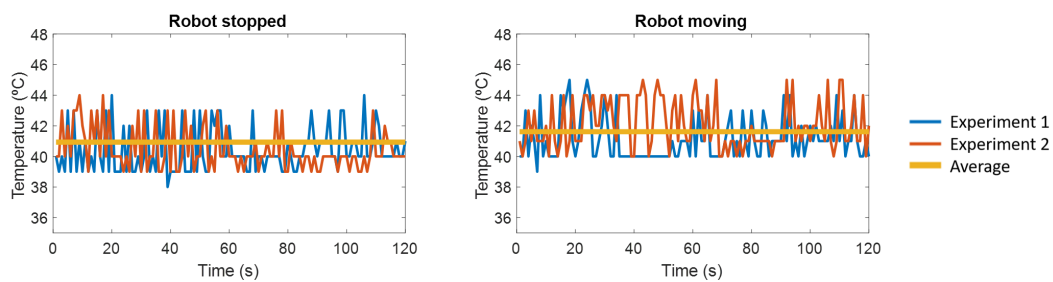
Figure 7. Multiple temperature measurements—room and object—and quad-rotor height from the floor acquired during a real-time flight versus the time.



Figure 8. Sequence of images obtained by the drone camera during the mobile ground robot test.

In order to have a reference value, the temperature inside the ground robot, as measured by its internal sensors was obtained, these sensor give a temperature of 40.9 °C when the robot was stopped and 41.6 °C when it was moving. The measurements obtained by the proposed system are presented in Figure 9. They show the measurements taken with the robot stopped and moving, as well as the previously mentioned reference values. The robot’s case was the surface area measured, as it

evacuates the heat generated by the electromechanical components of the robot (i.e., computer, sensors and motors).



**Figure 9.** Measurements of temperature of the ground robot during the test.

The heat provided by some of the additional components of the robot, is coherent with the fact that there are some of the temperature measurements detected by the drone while flying over the ground are higher than the average or reference value measured by the robot's computer. The exact values that it should measure cannot be determined without accurate models of the heat sources and transmitting materials in the robot. However, the collected data can explain the measurements obtained by sensors 7 and 10 during the flight, since the robot surface has a temperature between the ones inside the robot (40 °C to 42 °C) and around it (20 °C to 22 °C).

#### 4. Discussion and Conclusions

A novel temperature tracking concept oriented to energy efficiency management inside buildings is proposed in this paper. This tool is suitable to identify heat losses in industrial buildings, providing a key information to optimize the cooling management. This system is especially useful in large data centers with dozens of servers. The persistent temperature monitoring in those places, together with the adequate actions to improve the energy efficiency, will help to reduce the costs in millions of euros and contribute to a more sustainable planet.

The system proposed improves current state-of-the-art in mobile temperature tracking platforms, i.e., the thermal mapper [12]. This is possible because the sensing technology employed in ARSS improves the thermal mapper sensor response in 50%. Furthermore, the system proposed can achieve a maximum navigation speed around eight times higher than the speed from the mobile platform used in [12] ( $16 \frac{m}{s}$  versus  $2.2 \frac{m}{s}$ ). Additionally, this platform was developed to be cost/effort-effective providing many advantages in relation to conventional, and other merging thermography alternatives (see Table 1).

It was verified that the SW/HW decisions taken were appropriated for detecting temperature patches in real-time and without any random fluctuation in the readings. This conclusion is supported through a series of experiments (please refer to Section 3.2) conducted in an indoor setup.

The most important feature to validate was the viability of using the MLX90614 sensors for real-time temperature data acquisition from a flying UAV. It was additionally shown that a good relationship between distance-to-target and temperature readings can be achieved with the 10° FoV sensor. This feature might be important in applications where a secure flying distance is needed.

The ROI analysis provided in Appendix A shows that the initial investment of the proposed approach is less than that using fixed thermal cameras. It can be noticed that, over the years, there is an insurance factor that had not been considered in previous cases [20]. In any case, a company adopting these technologies is covered by some sort of insurance, which means that the small value that accumulates over the years could be discarded and summed up to the company insurance. Even though, it is important to take into account that the figures indicated in [20] are not precise regarding which cameras are used and how many. This could be crucial when dealing with large areas to be monitored. Therefore, initial investment can increase considerably in these cases. Finally, cameras also have a life-time and maintenance that is not specified.

This work proved that this combination of technologies is viable and that it can be further extended to other applications such as motion detection.

**Author Contributions:** Conceptualization, J.V.; methodology, J.V.; software, J.V., M.G., and J.J.R.; validation, J.V. and J.J.R.; formal analysis, J.V., M.G. and J.J.T.; investigation, J.V.; resources, J.V. and A.B.; data curation, J.V. and J.J.R.; writing—original draft preparation, J.V.; writing—review and editing, all; visualization, J.V.; supervision, J.V.; project administration, A.B.; funding acquisition, A.B.

**Funding:** The research leading to these results has received funding from the RoboCity2030-III-CM project (Robótica aplicada a la mejora de la calidad de vida de los ciudadanos. fase III; S2013/MIT-2748), funded by Programas de Actividades I+D en la Comunidad de Madrid and cofunded by Structural Funds of the EU.

**Acknowledgments:** The authors would like to thank to Roberto Valenti and Jizhong Xiao from the City College of New York for the fruitful discussion about aerial indoor navigation.

**Conflicts of Interest:** The authors declare no conflict of interest.

### Acronyms

<b>ARSS</b>	Aerial Remote Sensing System
<b>DO</b>	Distance from the Object
<b>FoV</b>	Field of View
<b>IMU</b>	Inertial Measurement Unit
<b>IR</b>	Infra-Red
<b>OL</b>	Object Length
<b>SC</b>	Sensor Coverage
<b>SW/HW</b>	Software-Hardware
<b>UAV</b>	Unmanned Aerial Vehicle

### Appendix A

The return of investment analysis is provided in Figure A1. This analysis was made based in the reports provide in [20]. It is clear from this analysis that hiring the service of a thermographer for providing thermography reports is much more expensive than the automated methods.

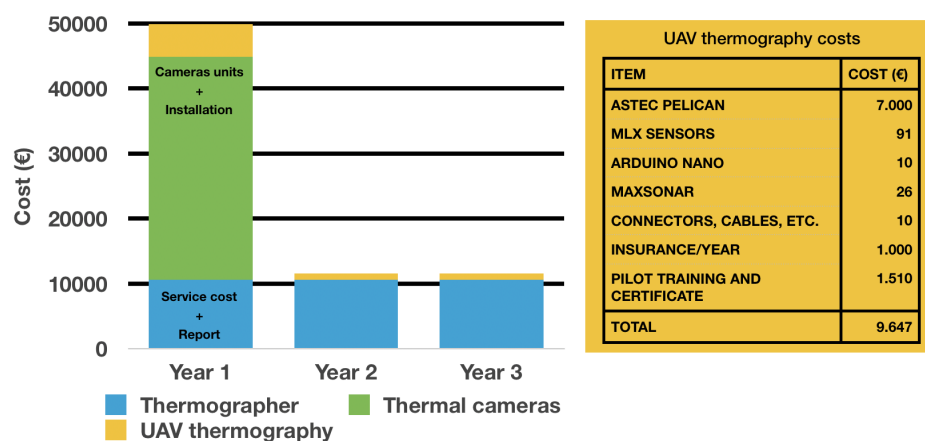


Figure A1. Return of investment (ROI) analysis.

### References

1. European Commission. *A Healthy and Sustainable Environment for Present and Future Generations*; The EU Explained; European Union: Brussels, Belgium, 2014.
2. Pachauri, R.K.; Meyer, L.; The Core Writing Team. *Climate Change 2014: Synthesis Report. Contribution of Working Groups I, II and III to the Fifth Assessment Report of the Intergovernmental Panel on Climate Change*; IPCC: Geneva, Switzerland, 2014; p. 151.

3. Council of European Union. Directive (EU) 2018/844 of the European Parliament and of the Council of 30 May 2018 Amending Directive 2010/31/EU on the Energy Performance of Buildings and Directive 2012/27/EU on Energy Efficiency, 2018. Available online: <http://data.europa.eu/eli/dir/2018/844/oj> (accessed on 20 January 2019).
4. Worrell, E.; Bernstein, L.; Roy, J.; Price, L.; Harnisch, J. Industrial energy efficiency and climate change mitigation. *Energy Effic.* **2008**, *2*, 109–123. [[CrossRef](#)]
5. Agudo, P.U.; Pajas, J.A.; Pérez-Cabello, F.; Redón, J.V.; Lebrón, B.E. The Potential of Drones and Sensors to Enhance Detection of Archaeological Cropmarks: A Comparative Study Between Multi-Spectral and Thermal Imagery. *Drones* **2018**, *2*, 29. [[CrossRef](#)]
6. Cowley, D.C.; Moriarty, C.; Geddes, G.; Brown, G.L.; Wade, T.; Nichol, C.J. UAVs in Context: Archaeological Airborne Recording in a National Body of Survey and Record. *Drones* **2018**, *2*, 2. [[CrossRef](#)]
7. Natesan, S.; Armenakis, C.; Benari, G.; Lee, R. Use of UAV-Borne Spectrometer for Land Cover Classification. *Drones* **2018**, *2*, 16. [[CrossRef](#)]
8. Zhang, J.; Jung, J.; Sohn, G.; Cohen, M. Thermal Infrared Inspection of Roof Insulation Using Unmanned Aerial Vehicles. *Int. Arch. Photogramm. Remote Sens. Spat. Inf. Sci.* **2015**, *40*, 381. [[CrossRef](#)]
9. González-Aguilera, D.; Lagüela, S.; Rodríguez-Gonzálvez, P.; Hernández-López, D. Image-based thermographic modeling for assessing energy efficiency of buildings façades. *Energy Build.* **2013**, *65*, 29–36. [[CrossRef](#)]
10. Hung, S.S.; Chang, C.Y.; Hsu, C.J.; Chen, S.W. Analysis of Building Envelope Insulation Performance Utilizing Integrated Temperature and Humidity Sensors. *Sensors* **2012**, *12*, 8987–9005. [[CrossRef](#)] [[PubMed](#)]
11. Vidas, S.; Moghadam, P.; Bosse, M. 3D thermal mapping of building interiors using an RGB-D and thermal camera. In Proceedings of the 2013 IEEE International Conference on Robotics and Automation (ICRA), Karlsruhe, Germany, 6–10 May 2013; pp. 2311–2318.
12. Borrmann, D.; Nüchter, A.; Dakulovic, M.; Maurovic, I.; Petrovic, I.; Osmankovic, D.; Velagic, J. The Project ThermalMapper—Thermal 3D Mapping of Indoor Environments for Saving Energy. In Proceedings of the 10th IFAC Symposium on Robot Control, Dubrovnik, Croatia, 5–7 September 2012; pp. 31–38.
13. Murphy, R.R. *Introduction to AI Robotics*, 1st ed.; MIT Press: Cambridge, MA, USA, 2000.
14. Chan, H.; Connell, J.; Isci, C.; Kephart, J.O.; Lenchner, J.; Mansley, C.; McIntosh, S. A Robot As Mobile Sensor and Agent in Data Center Energy Management. In Proceedings of the 8th ACM International Conference on Autonomic Computing, Karlsruhe, Germany, 14–18 Jun 2011; ACM: New York, NY, USA, 2011; pp. 165–166.
15. Van Geet, O. *Best Practices Guide for Energy-Efficient Data Center Design*; Federal Energy Management Program, U.S. Department of Energy: Washington, DC, USA, 2011.
16. Dryanovski, I.; Valenti, R.G.; Xiao, J. An open-source navigation system for micro aerial vehicles. *Auton. Robots* **2013**, *34*, 177–188. [[CrossRef](#)]
17. Kaplan, H. *Practical Applications of Infrared Thermal Sensing and Imaging Equipment*, 3rd ed.; SPIE Optical Engineering Press: Bellingham, WA, USA, 2007; p. 192.
18. Melexis Data Sheet. Available online: <https://www.melexis.com/-/media/files/documents/datasheets/mlx90614-datasheet-melexis.pdf> (accessed on 30 September 2018).
19. Quigley, M.; Conley, K.; Gerkey, B.; Faust, J.; Foote, T.; Leibs, J.; Wheeler, R.; Ng, A.Y. ROS: An open-source Robot Operating System. In Proceedings of the ICRA workshop on Open Source Software, Kobe, Japan, 12–17 May 2009; Volume 3, p. 5.
20. Automated vs. Manual Thermal Monitoring Return on Investment. Available online: <https://systemswithintelligence.com/wp-content/uploads/2017/07/Automated-vs-Manual-Thermal-Monitoring-Return-on-Investment-Apr1317.pdf> (accessed on 1 March 2019).

